Macromolecular Bioscience
www.mbs-journal.de

Porous Microstructured Surfaces with pH-Triggered Antibacterial Properties

*Adolfo del Campo, Coro Echeverría, Miguel San Martín, Rocío Cuervo-Rodríguez, Marta Fernández-García, and Alexandra Muñoz-Bonilla**

New antibacterial films are designed with the capability to reversibly regulate their killing and repelling functions in response to variations in environmental pH. These systems consist of porous polystyrene surfaces as the main components and a copolymer bearing pH-sensitive thiazole and triazole groups as the minor components. These pH-sensitive groups, located on the surfaces, can be partially protonated at acidic pH levels, increasing the positive charge density of the surfaces and their antibacterial activity. Similarly, their bacterial adhesion and killing efficiencies in response to changes in pH are evaluated by analyzing the bacterial viability of *Staphylococcus aureus* bacteria on the surfaces under acidic and neutral pH values. It is demonstrated that after only 1 h of incubation with the bacterial suspension in acidic conditions, the surfaces killed the bacteria, while at pH = 7.4, some of the adhered bacteria are removed. Furthermore, the surface topography exerts an important role by intensifying this response.

1. Introduction

Biomedical-device-associated infections due to bacterial adhesion and biofilm formation are a serious problem in human healthcare, causing high rates of mortality.[1,2] Of particular concern is the occurrence of infections related to implanted devices, including surgical site infections, urinary tract infections, central line-associated bloodstream infections, ventilator-associated pneumonia, and orthopedic implant-associated infections, which are currently the main postsurgical complications.[3–5] Therefore, the control and prevention of bacterial colonization on material surfaces are an urgent priority. A great number of strategies to tackle bacterial contamination have been developed over the past few decades. Polymeric coatings with antimicrobial properties have emerged as very efficient candidates to limit bacterial contamination, typically by employing two general approaches: the prevention of bacterial adhesion or the killing of adhered bacteria. Antifouling coatings, which typically include polymers based on poly(ethylene glycol)[6] or zwitterionic polymers,[7] are capable of effectively preventing the adhesion of bacteria for only a short time, because their surfaces can be degraded or masked by substances in physiological environments. The second major strategy is the creation of bactericidal surfaces, which act either through direct contact[8] or following active release strategies.[9] While biocide release surfaces can reduce adhesion and eliminate infections, they present several problems associated with side effects and toxicity, the appearance of antibiotic-resistant bacteria, and the depletion of active agents, requiring reloading steps. Alternatively, contact-killing surfaces in which antimicrobial components (commonly cationic materials) are attached onto the surfaces have also been widely investigated.[10,11] These surfaces exert efficient killing action without releasing biocides and avoid the limitations described above. The major drawback to these bactericidal surfaces is the accumulation of dead microorganisms on the surface, which reduces their efficiency. Dead bacteria not only diminish the biocidal activity by reducing contact but also offer a favorable environment for the adhesion of surrounding bacteria and contribute to the formation of biofilm.

Consequently, many efforts have been made to overcome these limitations by combining both killing and repelling functions on the same surface.[12–16] To enhance the performance of these surfaces with dual actions, investigators have focused on designing surfaces with the capacity to change between killing and antifouling actions under certain stimuli.[17,18] Accordingly, an ideal antimicrobial surface should prevent bacterial adhesion, kill adhered bacteria in case of contamination and, afterward, clean the surface of dead bacteria (i.e., demonstrate a self-cleaning capacity). Such smart surfaces should be capable of reversibly varying their surface properties in response to changes in the environment, such as local acidity, the presence of enzymes,[19] temperature,[20,21] light,[22,23] or the presence of counterions,[24,25] among others. Thus, by simple changes in the

Dr. A. del Campo
Instituto de Cerámica y Vidrio-Consejo Superior de Investigaciones Científicas (ICV-CSIC)
C/Kelsen 5, 28049 Madrid, Spain
Dr. C. Echeverría, M. San Martin, Dr. M. Fernández-García, Dr. A. Muñoz-Bonilla
Instituto de Ciencia y Tecnología de Polímeros-Consejo Superior de Investigaciones Científicas (ICTP-CSIC)
C/Juan de la Cierva 3, 28006 Madrid, Spain
E-mail: sbonilla@ictp.csic.es
Dr. R. Cuervo-Rodríguez
Facultad de Ciencias Químicas
Universidad Complutense de Madrid
Avenida Complutense s/n, Ciudad Universitaria, 28040 Madrid, Spain
The ORCID identification number(s) for the author(s) of this article can be found under https://doi.org/10.1002/mabi.201900127.

DOI: 10.1002/mabi.201900127

external conditions, the surfaces can kill adhered bacteria and, subsequently, shed dead bacteria from the surface, cleaning the surface and maintaining long-term antimicrobial activity. As for pH-responsive surfaces, some of them may be considered bacterial-responsive antimicrobial surfaces. Bacterial colonization and biofilm formation might imply variations in the pH; typically, the local environment becomes more acidic as biofilm is formed due to bacterial metabolism and the secretion of lactic acid.[26,27] Smart antibacterial surfaces based on pH-responsive polymers have taken advantage of this local acidity and are designed to kill the bacteria when the pH drops, releasing the dead bacteria at higher pH values. For this purpose, multifunctional surfaces are commonly prepared in which one component presents antifouling properties dependent on the pH, while other components exert biocidal activity.[28–31] In an interesting example, a hydrogel functionalized with carboxybetaine moieties has been prepared that can reversibly switch between zwitterionic and cationic forms, repelling and killing bacteria, respectively.[32]

Herein, we developed new pH-responsive antimicrobial surfaces with porous structures following a simple and straightforward approach using the breath figures method. This approach allows for the very rapid (1–2 min) preparation of microstructured films via a very simple methodology, by casting the solution onto the substrate under a humid atmosphere.[33–35] The porous antibacterial films were prepared by this approach from polymeric solutions composed of commercial polystyrene as the major component and a block copolymer, bearing thiazole and triazole groups, as the minor material. Due to the breath figures method, the hydrophilic and pH-sensitive thiazole and triazole groups spontaneously segregate toward the surface. Therefore, the surface chemistry can be modified by variations of pH, as the thiazole and triazole groups[36,37] shift from neutral at physiological pH to positively charged thiazolium and triazolium groups at acidic pH values (see **Scheme 1**). When the positive charge increases at the surface (acidic pH), their wettability and antimicrobial activity are augmented. On the other hand, the surface becomes more hydrophobic and interactions with negatively charged bacteria and proteins decrease at neutral pH. The introduction of porosity by the breath figures method could improve these effects.

2. Experimental Section

2.1. Materials

The block copolymer polystyrene-*b*-poly(4-(1-(2-(4-methylthiazol-5-yl)ethyl)-1*H*-1,2,3-triazol-4-yl)butyl methacrylate) (PS_{54}-*b*-$PTTBM_{23}$, M_n = 13 600 g mol^{-1}, M_w/M_n = 1.74) was synthesized via atom transfer radical copolymerization (ATRP) as previously described.[10,38] The ^{1}H NMR spectrum and gel permeation chromatography (GPC) curve are displayed in Figures S1 and S2, Supporting Information. High-molecular-weight polystyrene (PS, Aldrich, $M_w = 2.50 \times 10^5$ g mol^{-1}) was used as the polymeric matrix. The solvent chloroform ($CHCl_3$) was purchased from Scharlau. Trizma buffer solution (pH = 7.4), 2-(*N*-morpholino)ethanesulfonic acid (MES) buffer solution (pH = 5.5), and bovine serum albumin-fluorescein isothiocyanate conjugate (BSA-FITC) were purchased from Aldrich and used as received. Round glass coverslips of 12 mm diameter used as film supports were obtained from Ted Pella, Inc.

For the microbiological assays, sodium chloride solution (NaCl suitable for cell culture, BioXtra) and phosphate buffered saline (PBS) powder (pH = 7.4) were acquired from Aldrich. American Type Culture Collection (ATCC): Gram-positive *Staphylococcus aureus* (ATCC 29213) was used as the bacterial strain. The LIVE/DEAD BacLight Bacterial Viability Kit (L-7012) was purchased from Thermofisher Scientific.

2.2. Preparation of the Polymeric Coatings

Porous films were prepared by the breath figure method from blends consisting of a commercial polystyrene matrix with PS_{54}-*b*-$PTTBM_{23}$ copolymer as a minor component (5, 10, and

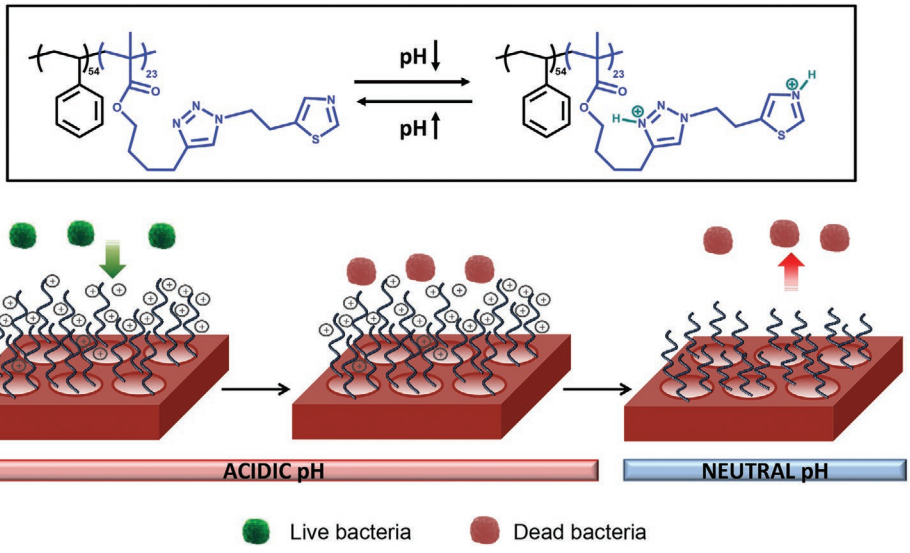

Scheme 1. Schematic illustration of the pH-responsive breath figures pattern.

20 wt%). Both polymers were dissolved in chloroform to total concentrations of polymers in solution of 15 or 30 mg mL^{-1}. From these solutions, 60 mm^2 films were prepared by casting 30 µL of the solution onto glass wafers (12 mm diameter) at room temperature under controlled relative humidity (RH) (60, 70, and 80%) inside a closed chamber.

2.3. Protein Adsorption Experiments

The prepared films were immersed in 0.5 mL of BSA-FITC solution (0.04 mg mL^{-1}) with either Trizma buffer solution at pH = 7.4 or MES buffer solution at pH = 5.5. The protein solutions were freshly prepared prior to use and analyzed by zeta potential measurements in a Malvern Zetasizer instrument. The films were incubated for 2 h at 25 °C and then removed from the solution. The unbound protein concentration in the resultant solution was then analyzed by fluorescence spectroscopy. For these measurements, 100 µL of each solution was placed in a 96-well round-bottom microplate. The fluorescence intensity of each well was measured using a Synergy HTX Multi-Mode Reader spectrophotometer (Bio-Tek) at an excitation wavelength of 480 nm and an emission wavelength of 525 nm. All films were analyzed in triplicate, and blank experiments were performed with the buffer solutions. The intensity data were converted to concentration of unbound protein using the corresponding standard curve, and finally, the amount of protein adsorbed onto the surfaces was calculated by subtracting the unbound concentration from the initial concentration (represented in ng cm^{-1}). Each measurement was collected at least three times.

2.4. Evaluation of Antimicrobial Activity in Films

The microorganisms *S. aureus* were grown on a 5% sheep blood Columbia agar plate over 24 h in an incubator at 37 °C (Jouan IQ050 incubator). Subsequently, bacteria were suspended in saline solution, and the concentration was adjusted to a turbidity equivalent of 0.5 McFarland turbidity standard (10^8 colony forming units [CFU] mL^{-1}). The optical density of the microorganism suspension was measured in a DensiCHEK Plus (VITEK, BioMérieux). Afterward, the suspension was adjusted to 10^6 CFU mL^{-1} with either PBS (pH = 7.4) or MES (pH = 5.5) buffer. Then, the films, supported on 12-mm-diameter glass wafers and previously sterilized by UV irradiation, were placed in a 24-well plate and incubated in 0.5 mL of the bacterial suspension in buffers (PBS and MES) at 37 °C for 1 h. After that, the bacterial suspensions were removed, and samples were washed three times with sterile water. The bacteria on the samples were stained using a LIVE/DEAD BacLight Viability Kit and fixed in 2.5% glutaraldehyde solution for 2 h. The surfaces were observed with a fluorescence microscope (Nikon Eclipse TE2000-5) combined with a digital Nikon DS-Ri2 camera. The fluorescence images were analyzed using ImageJ software. The killing efficiency was determined by dividing the area of dead bacteria by the total area of both live and dead bacteria. The analysis was performed at least in triplicate.

2.5. Characterization

Scanning electron microscopy (SEM) images of the surfaces were taken using a Philips XL30 with an acceleration voltage of 25 kV. The films were coated with gold prior to scanning. The chemical composition and distribution of the different blend components on the films were analyzed using confocal Raman microscopy on a CRM-Alpha 300 RA microscope (WITec, Ulm, Germany) equipped with an Nd:YAG laser (maximum power output of 50 mW at 532 nm). Water contact angle measurements of the prepared films were carried out in a KSV Theta goniometer (KSV Instruments Ltd., Finland) from digital images of 3.0-µL water droplets on the surfaces. Prior to measurements at a given pH value, films were pretreated with the corresponding buffer solution. All samples were measured in triplicate, and the average values ± SD (standard deviation) are presented.

3. Results and Discussion

3.1. Preparation and Characterization of Microstructured Surfaces Functionalized with Antimicrobial Polymers

Porous films functionalized with the antimicrobial copolymer PS_{54}-*b*-$PTTBM_{23}$ were prepared by the breath figures approach using chloroform as the solvent. In previous works, cationic copolymers with permanent positive charges, such as polymers with quaternary ammonium groups, have been employed to incorporate antimicrobial properties into breath figure films.[39,40] However, polar solvents such as THF, which produce poorly ordered structures, and/or polymers with low charge density are required in most cases in order to solubilize the cationic polymers. In the current work, we prepared films from a neutrally charged polymer, PS_{54}-*b*-$PTTBM_{23}$; thus, typical organic solvents used in the breath figures approach can be employed. This block copolymer is composed of a PTTBM block with two groups per monomeric unit (thiazole and triazole groups) susceptible of quaternization or protonation at acidic pH values (see Scheme 1), which would lead to the breath figures films having highly charged surfaces.

Chloroform solutions of blends, composed of a commercial PS matrix with the copolymer as a minor component, were cast onto glass substrates under controlled humidity. The relative humidity and composition of the blend were varied, as they are important parameters that strongly influence the formation of porous films in this approach. First, the effect of humidity on the formed micropatterns was evaluated. As observed in **Figure 1**, for a film containing 10 wt% copolymer, flat surfaces were obtained when the humidity was 60% during film formation, whereas porous surfaces with multiple-porosity appear at higher humidity levels of 70% and 80%. The size of the pores increases as the relative humidity (RH) rises during the film preparation, as previously observed in other systems found in the literature,[33,34,41] with diameters of 2.9 ± 0.4 µm and 3.5 ± 0.8 µm for the films prepared at 70% and 80% RH, respectively. Additionally, **Figure 2** shows the SEM images of the films obtained from varied contents

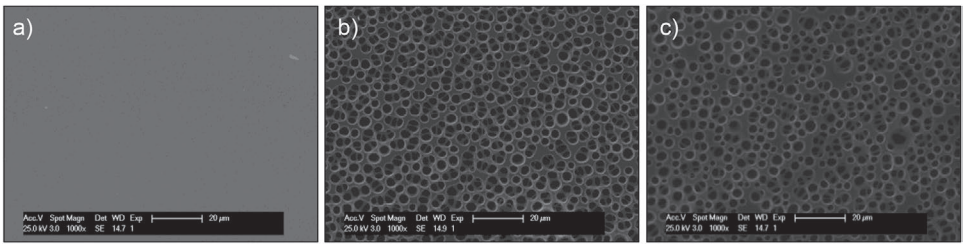

Figure 1. SEM images of films prepared by the breath figures approach from chloroform solution (30 mg mL^{-1}) with a PS/PS_{54}-*b*-$PTTBM_{23}$ ratio of 90/10 wt% at different % relative humidity (RH): a) 60%, b) 70%, and c) 80%.

of PS_{54}-*b*-$PTTBM_{23}$ copolymer in the blend at 70% humidity. It is clearly observed that the regularity of the porous microstructure is significantly reduced with the addition of the copolymer. The film composed of commercial polystyrene exhibits the honeycomb pattern typically found by the breath figures approach, while films containing the block copolymer at 5, 10, and 20 wt% become more irregular, with multiple-porosity and multilayer structures (see Figure S3, Supporting Information). Interestingly, two levels of porosity are obvious on the surface, which is relatively homogeneous in the film with 10 wt% of copolymer (Figure 2c).

As expected, the incorporation of the amphiphilic copolymer into the polystyrene matrix strongly influences the surface topography of the films. In the breath figures process, amphiphilic structures tend to arrange around the water droplets that condense at the air/solution interface, with hydrophilic groups in contact with the water. This leads to the preferential location of the hydrophilic moieties toward the interface inside the cavities once the solvent is evaporated, and a porous pattern is formed.[33,41,42] Furthermore, when a polymer blend is used, the hydrophilic or amphiphilic components of the blend might segregate to the walls of the pores.[43,44] Here, the spatial distribution at the film surface of the two components of the blend, the PS_{54}-*b*-$PTTBM_{23}$ copolymer and the polystyrene matrix, was further analyzed by Raman confocal microscopy. The Raman micrographs displayed in **Figure 3** were taken point by point with a step of 100 nm and performed using the ring breathing mode associated with PS at 1012 cm^{-1} Raman shift (red areas) and the signal at 1738 cm^{-1} assigned to the carbonyl groups of the PS_{54}-*b*-$PTTBM_{23}$ copolymer (blue regions). In effect, the Raman micrographs corroborate that the amphiphilic copolymer is mainly segregated toward the wall of the pores.

Therefore, we can confirm that the PS_{54}-*b*-$PTTBM_{23}$ copolymer is mainly located in the cavities of the breath figures pattern.

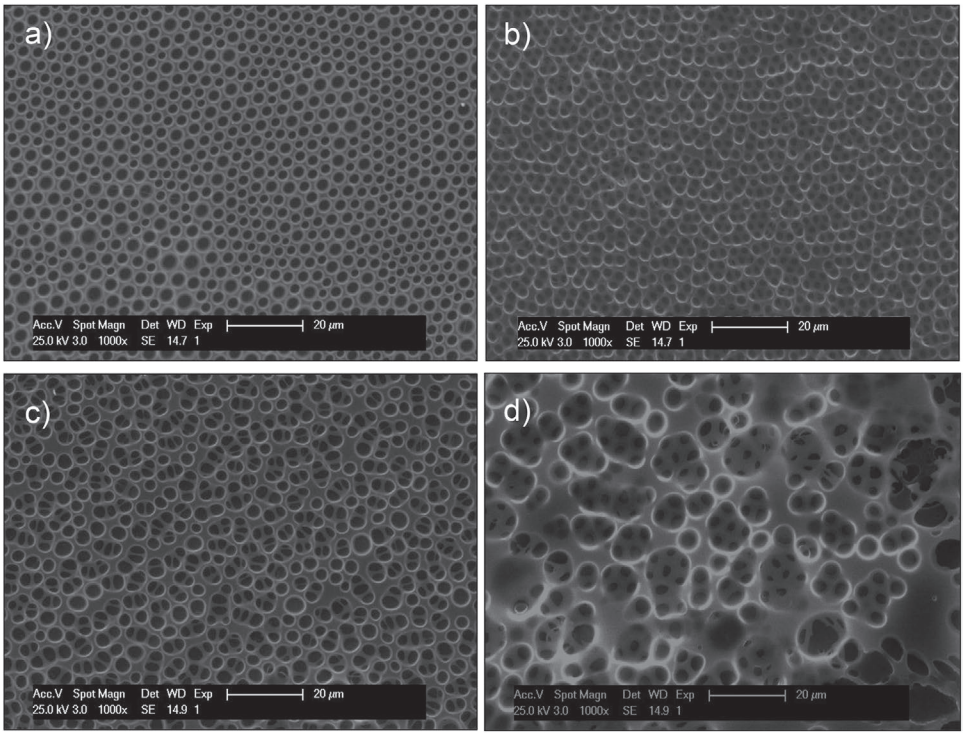

Figure 2. SEM images of films prepared by the breath figures approach at 70% relative humidity from chloroform solution (30 mg mL^{-1}) containing commercial polystyrene and a) 0, b) 5, c) 10, or d) 20 wt% of PS_{54}-*b*-$PTTBM_{23}$ copolymer.

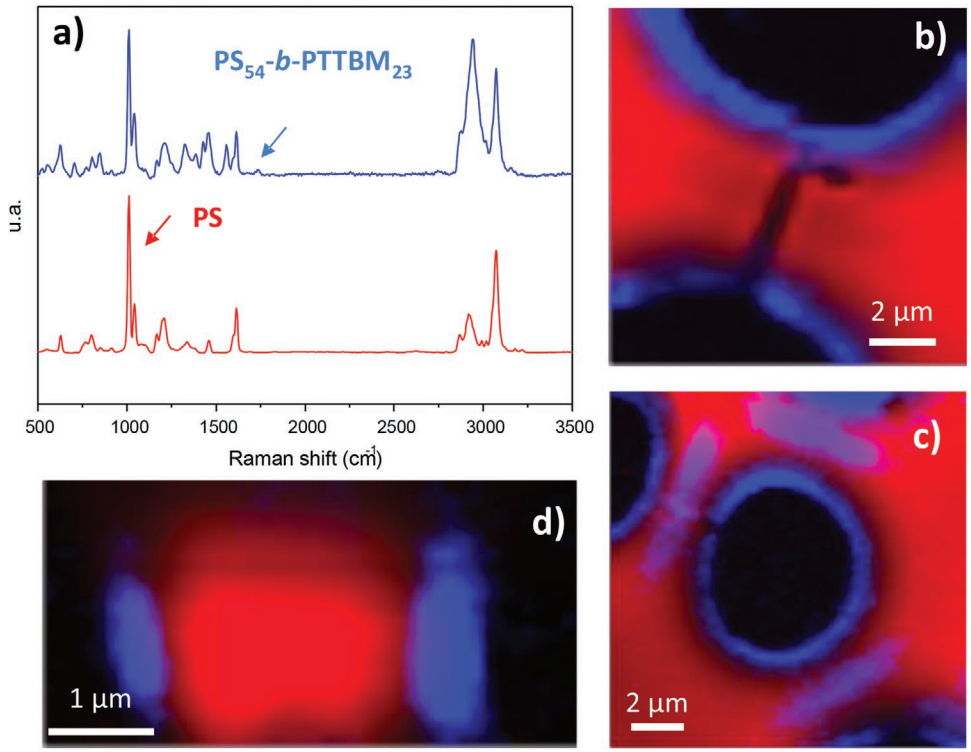

Figure 3. Raman micrographs of a polymer blend film prepared at 70% relative humidity from chloroform solution (30 mg mL^{-1}) with a PS/PS_{54}-*b*-$PTTBM_{23}$ ratio of 90/10 wt%. a) Average Raman spectra of the pure commercial PS and PS_{54}-*b*-$PTTBM_{23}$ copolymer, and the corresponding maps b,c) XY maps, d) XZ map (cross section). Red areas represent a high intensity of the signal at 1012 cm^{-1} assigned to PS, thus evidencing the presence of PS-rich spaces, whereas blue areas indicate a high intensity of the 1738 cm^{-1} signal associated with the carbonyl groups of PS_{54}-*b*-$PTTBM_{23}$ copolymer.

3.2. Surface Properties in Response to Changes in pH

The surface wettability of the micropatterned surfaces under different pH values, 7.4 and 5.5, was investigated to evaluate their pH-responsive behavior. **Figure 4** shows the contact angle values of the films pretreated by buffer solutions at both pH levels. Only films with 0, 5, and 10 wt% were investigated as the sample with the highest content of copolymer, 20 wt%, exhibited a highly irregular pattern.

From these data, it is clearly observed that the microstructured films prepared by the breath figures approach at 70 and 80% RH showed higher contact angle values at both pH levels in comparison with the flat surfaces obtained at 60% RH. This is expected because the films are composed mainly of PS and,

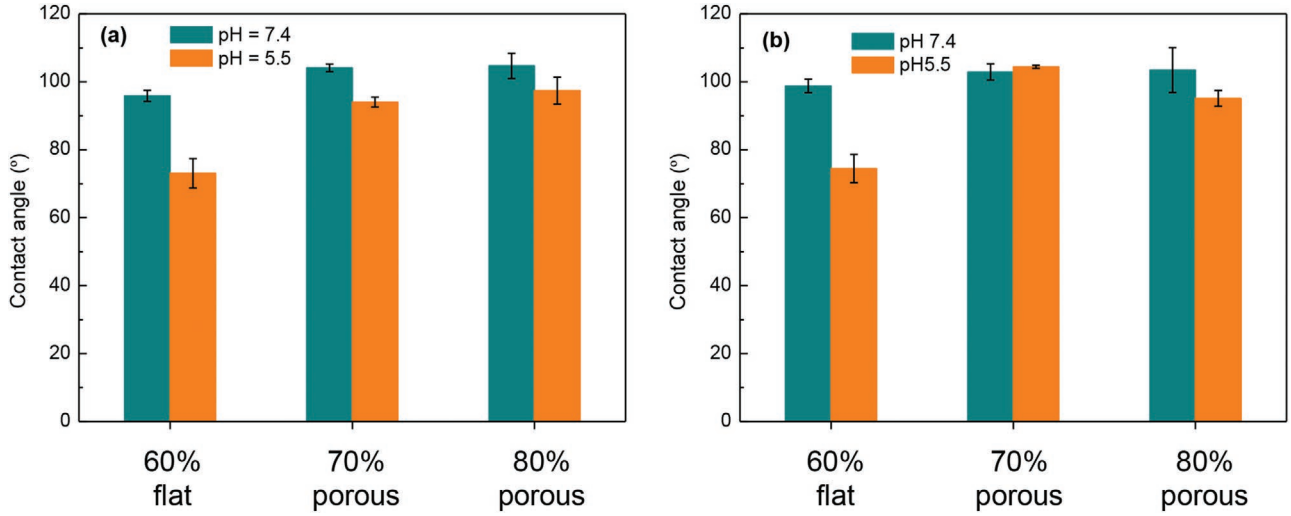

Figure 4. Water contact angles of the films prepared at different relative humidities of 60%, 70%, and 80%, and pretreated with buffer solutions at pH = 7.4 and 5.5. Samples obtained with a PS/PS_{54}-*b*-$PTTBM_{23}$ ratio of a) 95/5 wt% and b) 90/10 wt%.

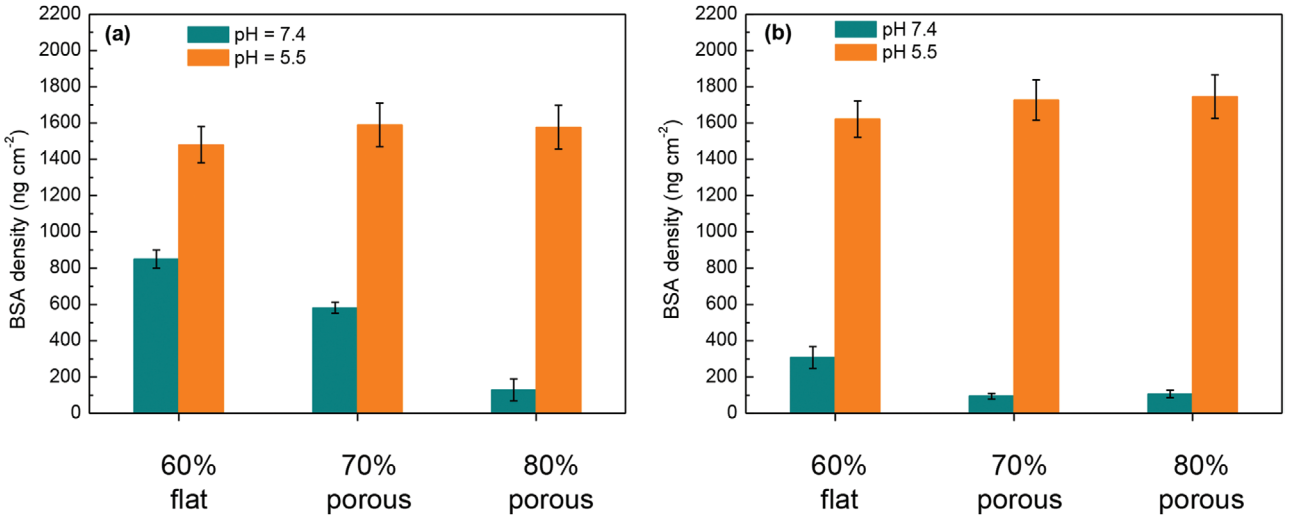

Figure 5. Surface density of BSA on films prepared at different % relative humidities, 60%, 70%, and 80%, and pretreated by buffer solutions at pH = 7.4 and 5.5. Samples obtained with a PS/PS_{54}-*b*-$PTTBM_{23}$ ratio of a) 95/5 wt% and b) 90/10 wt%.

according to Wenzel's equation, roughness increases the contact angle for low-energy hydrophobic surfaces.[35] Independently of this, the surface wettability, in general, slightly improves at acidic pH, proving the presence of the pH-responsive copolymer at the surface. When decreasing the pH, the equilibrium shifts toward thiazolium and triazolium groups (Scheme 1), increasing the positive charge density of the surface and thus enhancing the wettability. Nevertheless, these variations in wettability with pH are not as large as expected, because the contact angle is strongly influenced by the topography. Therefore, we see that both the topography and the pH-tunable surface chemistry influence the wettability of the prepared films.

To further assess the pH-responsive behavior of the porous films containing the PS_{54}-*b*-$PTTBM_{23}$ copolymer, protein adsorption experiments were performed using BSA as a model protein. This protein presents a negative net charge at neutral and slightly acidic pH and can electrostatically interact with the positive charges at the surface of the films. In fact, zeta potential measurements of the aqueous solution of BSA at both pH values reveal values of −22.2 mV and −10.6 mV, at pH = 7.4 and 5.5, respectively. Hence, the prepared films were immersed into a FITC-labeled BSA solution for 2 h, and the protein adsorbed on the films was indirectly quantified by analyzing the unbound BSA of the resultant solution. **Figure 5** displays the surface density of BSA for all prepared films under both pH values.

As expected, the amount of BSA adsorbed on the surfaces is much higher when the pH of the solution is acidic (5.5), as a result of the protonation of the thiazole and triazole groups, which leads to positive charges and favors electrostatic interactions between the BSA and surface. The surface density of BSA is slightly superior in films with higher copolymer contents, shown in Figure 5b, which in turn have higher contents of positive charges. Remarkably, this adsorption of BSA at pH = 5.5 improves in the microstructured films, prepared at 70% and 80% RH, probably due to the better accessibility of the cationic groups, which are segregated toward the cavities of the pattern as demonstrated by Raman confocal microscopy. In contrast, at pH = 7.4, the adsorption of BSA on the surfaces is significantly limited in all films, and interestingly, the surface density of BSA decreases in the microstructured films. At pH = 7.4, the equilibrium is shifted to deprotonated forms, so the films present lower positive charges. Thus, less electrostatic interaction with the negatively charged BSA is expected. The topography also exerts an effect on the nonspecific BSA adsorption at pH = 7.4. The incorporation of micropores on the surface is concomitant with an increase in the content of neutrally charged hydrophilic copolymer at the surface, which reduces the adsorption of proteins due to the hydrophilic effect.

Therefore, these surfaces demonstrated pH-responsive properties, exhibiting low nonspecific protein adsorption at physiological pH, while electrostatically interacting with negatively charged biomolecules at an acidic pH. It is worth mentioning that the porous structures intensify the adsorption-repelling effects in comparison with flat surfaces because in porous films, the copolymer is segregated toward the surface as a result of the breath figures approach, making more pH-sensitive groups available at the surface.

3.3. Bacterial Attachment and Killing Efficiency in Response to Changes in pH

The obtained porous surfaces have been demonstrated to reversibly vary their physicochemical properties in response to changes in pH by variations in the positive charges of the amphiphilic copolymers located in the pores. Many contact-killing antimicrobial surfaces are based on interfaces functionalized with cationic charges, which electrostatically interact with the negatively charged bacterial membrane to cause wall rupture, cell lysis, and bacterial death. However, these traditional surfaces are often active for only a short time period, as the accumulation of dead bacteria diminishes the biocidal activity. Therefore, an ideal antimicrobial surface should shed dead bacteria to clean its surface. Here, we expect that the copolymers segregated at the surface would be active in attaching and killing bacteria at an acidic pH, as the chains will be positively

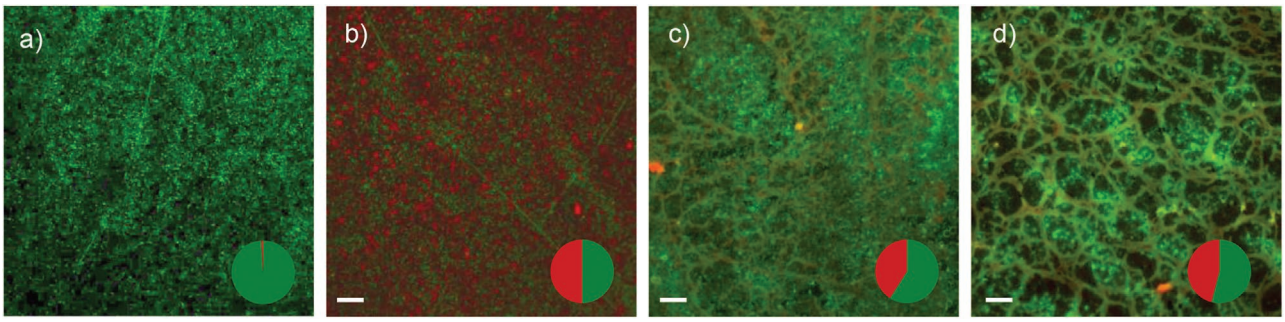

Figure 6. Representative fluorescence images of *S. aureus* attachment under pH 5.5 buffer solutions on surfaces of: a) PS obtained at 60% RH (flat); b) PS/PS_{54}-*b*-$PTTBM_{23}$ blends with a 90/10 wt% ratio obtained at 60% RH (flat); c) PS/PS_{54}-*b*-$PTTBM_{23}$ blends with a 90/10 wt% ratio obtained at 70% RH (porous); and d) PS/PS_{54}-*b*-$PTTBM_{23}$ blends with a 90/10 wt% ratio obtained at 80% RH (porous). Samples were incubated in bacterial suspension for 1 h followed by the live/dead staining protocol. Green staining indicates live bacteria, and red staining indicates dead bacteria. Inset diagrams in the lower right corners present the percentage of live (in green) and dead (in red) bacteria. Scale bar is 100 µm.

charged; at neutral pH, this charge density and the resultant interactions with the bacterial membranes decrease, leading to the release of dead bacteria. To assess whether acidic pH activates the biocidal function of the coatings, we investigated the bacterial viability of cells attached onto the surfaces under acidic (pH = 5.5) conditions using *S. aureus* as a model bacteria. The different films, both flat surfaces obtained at 60% RH and microstructured surfaces obtained at 70% and 80% RH, were incubated in bacterial suspension buffer at 37 °C for 1 h. After washing the samples, the viability of bacteria attached on the surfaces was determined by a standard live/dead staining assay. Microphotographs displayed in **Figure 6** clearly show red fluorescence, indicating cell death. This is due to the partial protonation of the thiazole and triazole groups of the copolymers located on the surface, which generates positive charges. As a control experiment, a polystyrene film without the copolymer did not show the bactericidal effect activated by pH (Figure 6a).

No significant differences in the killing efficiency, considering the killing percentage, can be observed between the tested films under similar conditions, whether flat or porous surfaces (**Figure 7**a). However, the attachment of bacteria on the surface of the films differs considerably on porous surfaces in comparison with flat films. Figure 7b represents the bacterial coverage determined from the fluorescence images. It is clearly observed that in porous surfaces, the adhesion is considerably higher than in flat films, as expected by the fact that the content of block copolymer at the interface is larger. In addition, whereas on flat films the bacteria adhere to the surface almost individually, on porous surfaces, the bacteria tend to gather, as seen in Figure 6 and Figure S4, Supporting Information (optical image). This aggregation has been previously observed in patterned films with small pores; bacteria could form a biofilm on the top surface because individual bacteria accumulate and stabilize around the pores, and the area coverage by bacteria dramatically increases.[45] Thus, we can confirm that the bacteria surface coverage at acidic pH is higher in porous surfaces compared to the flat control surface, which leads to a greater number of dead bacteria.

Next, the bacteria-releasing capability of these surfaces was evaluated by incubating the films, previously treated at pH = 5.5, in a buffer solution at pH = 7.4 for 1 h. As shown in Figure 7b, the percentage of bacterial coverage decreases, meaning that the films are able to release a high number of

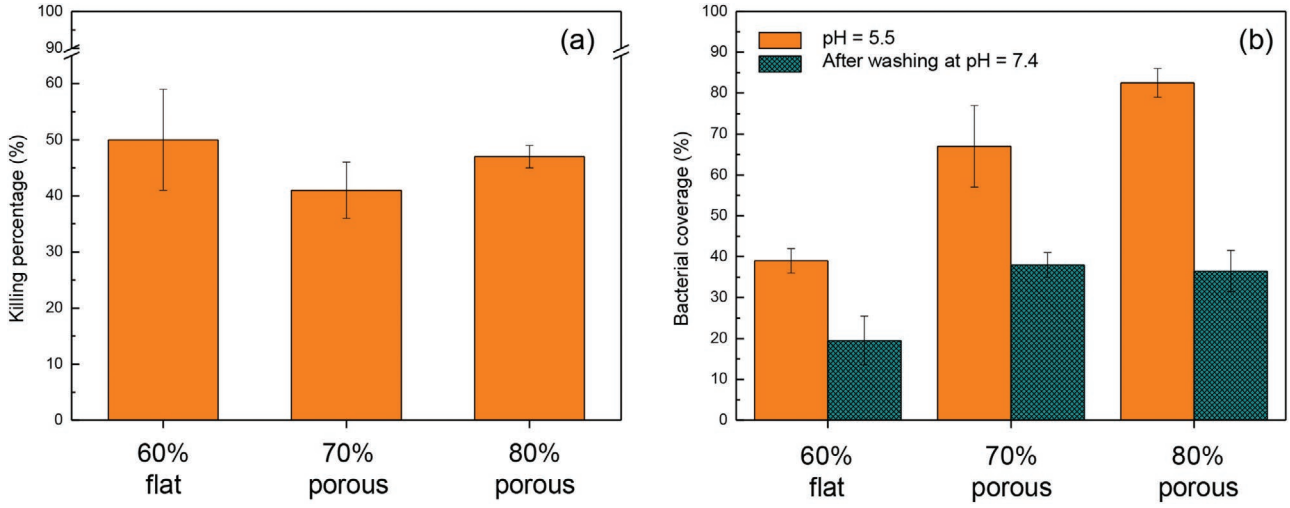

Figure 7. Comparison of the a) killing percentages and b) bacterial coverages of the films incubated in bacterial suspension for 1 h at pH = 5.5 and after a washing step at pH = 7.4.

bacteria, although a relatively high percentage of bacteria is still retained (20–35%).

These results demonstrate that the antimicrobial surfaces are capable of killing bacteria at an acidic pH and releasing a portion of the dead bacteria when the pH becomes neutral. Furthermore, in this case, the porosity at the surface induced by the breath figures approach intensifies both effects.

4. Conclusions

In summary, we have developed new smart antimicrobial surfaces based on the protonation–deprotonation equilibrium of thiazole and triazole groups as a function of environmental pH. These surfaces were prepared by a very simple and straightforward approach, the breath figures method, from polymer blend solutions; this method introduces porosity and segregates the amphiphilic and pH-sensitive copolymer at the surfaces toward the pores. The pH-responsive properties of the resulting surfaces have been demonstrated, including low wettability and low protein adsorption at neutral pH and enhanced wettability and electrostatic interactions with negatively charged BSA protein at acidic pH. The microstructures on the surface improve the adsorption of BSA at acidic pH while diminishing this adsorption at neutral pH in comparison with the control flat film. The antimicrobial surfaces obtained also show a capacity for killing bacteria at acidic pH, allowing the partial removal of dead bacteria when the pH returns to neutral. The effectiveness of these surfaces as antibacterial and self-defensive coatings is improved for porous surfaces in comparison with flat films. Finally, due to the versatility of the breath figures technique, these systems could also be improved by rational design, modification of the pore size, and the incorporation of additional functionalities. Therefore, this approach provides a proof of concept to develop new strategies to engineer smart surfaces with switchable antimicrobial and releasing properties.

Supporting Information

Supporting Information is available from the Wiley Online Library or from the author.

Acknowledgements

This work was supported financially by the MINECO (Project MAT2016-78437-R and Project MAT2017-86450-C4-1-R), the Agencia Estatal de Investigación (AEI, Spain), and Fondo Europeo de Desarrollo Regional (FEDER, EU) and by CSIC (Project 201760I064). C.E. also acknowledges MINECO for her IJCI-2015-26432 contract.

Conflict of Interest

The authors declare no conflict of interest.

Keywords

antibacterial coatings, breath figures, pH-responsive, porous films

Received: April 11, 2019
Revised: June 15, 2019
Published online: July 3, 2019

[1] I. Francolini, G. Donelli, *FEMS Immunol. Med. Microbiol.* **2010**, *59*, 227.
[2] B. Gottenbos, H. J. Busscher, H. C. Van der Mei, P. Nieuwenhuis, *J. Mater. Sci.: Mater. Med.* **2002**, *13*, 717.
[3] D. Campoccia, L. Montanaro, C. R. Arciola, *Biomaterials* **2006**, *27*, 2331.
[4] J. A. Al-Tawfiq, P. A. Tambyah, *J. Infect. Public Health* **2014**, *7*, 339.
[5] S. L. Percival, L. Suleman, C. Vuotto, G. Donelli, *J. Med. Microbiol.* **2015**, *64*, 323.
[6] S. Lowe, N. M. O'Brien-Simpson, L. A. Connal, *Polym. Chem.* **2015**, *6*, 198.
[7] G. Cheng, G. Li, H. Xue, S. Chen, J. D. Bryers, S. Jiang, *Biomaterials* **2009**, *30*, 5234.
[8] R. Kaur, L. Song, *Prog. Surf. Sci.* **2016**, *91*, 136.
[9] E. M. Hetrick, M. H. Schoenfisch, *Chem. Soc. Rev.* **2006**, *35*, 780.
[10] R. Cuervo-Rodriguez, F. Lopez-Fabal, J. L. Gomez-Garces, A. Munoz-Bonilla, M. Fernandez-Garcia, *Macromol. Biosci.* **2017**, *17*, 1700258.
[11] P. Elena, K. Miri, *Colloids Surf., B* **2018**, *169*, 195.
[12] B. L. Wang, K. F. Ren, H. Chang, J. L. Wang, J. Ji, *ACS Appl. Mater. Interfaces* **2013**, *5*, 4136.
[13] Q. Yu, Z. Wu, H. Chen, *Acta Biomater.* **2015**, *16*, 1.
[14] M. Salwiczek, Y. Qu, J. Gardiner, R. A. Strugnell, T. Lithgow, K. M. McLean, H. Thissen, *Trends Biotechnol.* **2014**, *32*, 82.
[15] X. Ding, S. Duan, X. Ding, R. Liu, F.-J. Xu, *Adv. Funct. Mater.* **2018**, *28*, 1802140.
[16] M. Kurowska, V. T. Widyaya, A. Al-Ahmad, K. Lienkamp, *Materials* **2018**, *11*, 1411.
[17] T. Wei, Z. Tang, Q. Yu, H. Chen, *ACS Appl. Mater. Interfaces* **2017**, *9*, 37511.
[18] X. Li, B. Wu, H. Chen, K. Nan, Y. Jin, L. Sun, B. Wang, *J. Mater. Chem. B* **2018**, *6*, 4274.
[19] G. Cado, R. Aslam, L. Séon, T. Garnier, R. Fabre, A. Parat, A. Chassepot, J.-C. Voegel, B. Senger, F. Schneider, Y. Frère, L. Jierry, P. Schaaf, H. Kerdjoudj, M.-H. Metz-Boutigue, F. Boulmedais, *Adv. Funct. Mater.* **2013**, *23*, 4801.
[20] B. Wang, Q. Xu, Z. Ye, H. Liu, Q. Lin, K. Nan, Y. Li, Y. Wang, L. Qi, H. Chen, *ACS Appl. Mater. Interfaces* **2016**, *8*, 27207.
[21] B. Wang, Z. Ye, Q. Xu, H. Liu, Q. Lin, H. Chen, K. Nan, *Biomater. Sci.* **2016**, *4*, 1731.
[22] W. Zhan, T. Wei, L. Cao, C. Hu, Y. Qu, Q. Yu, H. Chen, *ACS Appl. Mater. Interfaces* **2017**, *9*, 3505.
[23] T. Wei, W. Zhan, Q. Yu, H. Chen, *ACS Appl. Mater. Interfaces* **2017**, *9*, 25767.
[24] C. J. Huang, Y. S. Chen, Y. Chang, *ACS Appl. Mater. Interfaces* **2015**, *7*, 2415.
[25] Y.-S. Dong, X.-H. Xiong, X.-W. Lu, Z.-Q. Wu, H. Chen, *J. Mater. Chem. B* **2016**, *4*, 6111.
[26] H. S. Lee, S. S. Dastgheyb, N. J. Hickok, D. M. Eckmann, R. J. Composto, *Biomacromolecules* **2015**, *16*, 650.
[27] S. Pavlukhina, Y. Lu, A. Patimetha, S. Sukhishvili, *Biomacromolecules* **2010**, *11*, 3448.
[28] S. Yan, H. Shi, L. Song, X. Wang, L. Liu, S. Luan, Y. Yang, J. Yin, *ACS Appl. Mater. Interfaces* **2016**, *8*, 24471.
[29] T. Wei, Q. Yu, W. Zhan, H. Chen, *Adv. Healthcare Mater.* **2016**, *5*, 449.
[30] I. Zhuk, F. Jariwala, A. B. Attygalle, Y. Wu, M. R. Libera, S. A. Sukhishvili, *ACS Nano* **2014**, *8*, 7733.

[31] B. Wang, H. Liu, Z. Wang, S. Shi, K. Nan, Q. Xu, Z. Ye, H. Chen, *J. Mater. Chem. B* **2017**, *5*, 1498.
[32] B. Cao, Q. Tang, L. Li, J. Humble, H. Wu, L. Liu, G. Cheng, *Adv. Healthcare Mater.* **2013**, *2*, 1096.
[33] A. Muñoz-Bonilla, M. Fernández-García, J. Rodríguez-Hernández, *Prog. Polym. Sci.* **2014**, *39*, 510.
[34] U. H. F. Bunz, *Adv. Mater.* **2006**, *18*, 973.
[35] S. Chen, S. Gao, J. Jing, Q. Lu, *Adv. Healthcare Mater.* **2018**, *7*, 1701043.
[36] B. Schulze, U. S. Schubert, *Chem. Soc. Rev.* **2014**, *43*, 2522.
[37] Z. Song, R. A. Mansbach, H. He, K. C. Shih, R. Baumgartner, N. Zheng, X. Ba, Y. Huang, D. Mani, Y. Liu, Y. Lin, M. P. Nieh, A. L. Ferguson, L. Yin, J. Cheng, *Nat. Commun.* **2017**, *8*, 92.
[38] R. Tejero, D. López, F. López-Fabal, J. L. Gómez-Garcés, M. Fernández-García, *Polym. Chem.* **2015**, *6*, 3449.
[39] N. Vargas-Alfredo, A. Santos-Coquillat, E. Martinez-Campos, A. Dorronsoro, A. L. Cortajarena, A. Del Campo, J. Rodriguez-Hernandez, *ACS Appl. Mater. Interfaces* **2017**, *9*, 44270.
[40] A. Munoz-Bonilla, R. Cuervo-Rodriguez, F. Lopez-Fabal, J. L. Gomez-Garces, M. Fernandez-Garcia, *Materials* **2018**, *11*, 1266.
[41] K. H. Wong, T. P. Davis, C. Barner-Kowollik, M. H. Stenzel, *Polymer* **2007**, *48*, 4950.
[42] S. Yunus, A. Delcorte, C. Poleunis, P. Bertrand, A. Bolognesi, C. Botta, *Adv. Funct. Mater.* **2007**, *17*, 1079.
[43] A. S. de Leon, A. del Campo, M. Fernandez-Garcia, J. Rodriguez-Hernandez, A. Munoz-Bonilla, *Langmuir* **2012**, *28*, 9778.
[44] A. Del Campo, A. S. de Leon, J. Rodriguez-Hernandez, A. Munoz-Bonilla, *Langmuir* **2017**, *33*, 2872.
[45] K. Manabe, S. Nishizawa, S. Shiratori, *ACS Appl. Mater. Interfaces* **2013**, *5*, 11900.